

New Structural Picture of the $\text{Ge}_2\text{Sb}_2\text{Te}_5$ Phase-Change Alloy

X. Q. Liu,¹ X. B. Li,² L. Zhang,¹ Y. Q. Cheng,³ Z. G. Yan,¹ M. Xu,³ X. D. Han,^{1,*} S. B. Zhang,^{2,4,†} Z. Zhang,^{1,5} and E. Ma^{3,‡}

¹*Institute of Microstructure and Property of Advanced Materials, Beijing University of Technology, Beijing 100022, China*

²*State Key Laboratory on Integrated Optoelectronics, College of Electronic Science and Engineering, Jilin University, Changchun 130012, China*

³*Department of Materials Science and Engineering, Johns Hopkins University, Baltimore, Maryland 21218, USA*

⁴*Department of Physics, Applied Physics, and Astronomy, Rensselaer Polytechnic Institute, Troy, New York 12180, USA*

⁵*State Key Laboratory of Silicon Materials and Department of Materials Sciences and Engineering, Zhejiang University, 38 Zheda Road, Hangzhou 310027, China*

(Received 11 August 2010; published 13 January 2011)

Using electron microscopy and diffraction techniques, as well as first-principles calculations, we demonstrate that as much as 35% of the total Ge atoms in the cubic phase of $\text{Ge}_2\text{Sb}_2\text{Te}_5$ locate in tetrahedral environments. The Ge-vacancy interactions play a crucial stabilizing role, leading to Ge-vacancy pairs and the sharing of vacancies that clusters tetrahedral Ge into domains. The $\text{Ge}_2\text{Sb}_2\text{Te}_5$ structure with coexisting octahedral and tetrahedral Ge produces optical and structural properties in good agreement with experimental data and explains the property contrast as well as the rapid transformation in this phase-change alloy.

DOI: 10.1103/PhysRevLett.106.025501

PACS numbers: 61.66.Dk, 61.50.Ah, 64.70.Nd

The rapid and reversible phase transitions in phase-change materials (PCMs) are the basis of many volatile and nonvolatile memory devices [1–3]. As a prototype PCM, the $\text{Ge}_2\text{Sb}_2\text{Te}_5$ (GST) alloy has attracted considerable attention due to its high switching rate and extremely good reversibility [4,5]. The GST has two crystalline states: a metastable cubic phase (*c*-GST) [6–8] and a stable trigonal phase [9]. The reversible transition between the cubic and amorphous phases is exploited for memory and data storage. As recently pointed out by Wuttig *et al.*, the *c*-GST has a unique atomic and electronic structure, and hence special properties, and is largely responsible for the unusual phase change and property contrast [10]. A thorough understanding of the *c*-GST structure therefore holds the key for understanding the electronic properties and ultrafast phase transition of PCMs and the development of faster and more reliable PCMs [11–17].

The generally accepted picture is that the *c*-GST can be approximated as a distorted rocksalt (RS) structure. However, the atomic positions of the Ge atoms remain controversial. Powder x-ray diffraction suggests an octahedral-like (*o*-) environment for Ge [6,7], consistent with the RS structure, whereas x-ray fluorescence holography shows the Ge taking the tetrahedral symmetry (*t*-) [8]. Another important structural characteristic of *c*-GST is the presence of a large number of cation vacancies (CVs) [6,7,18]. It remains unsettled whether the CVs distribute randomly on the cation sublattice [6,7,18] or organize in some orderly fashion [17]. CVs have been suggested to play an important role in controlling the stability and the rapid phase change of GST [19–21].

In this work, we have developed a new understanding of the structure of the *c*-GST. In particular, using

(aberration-corrected) high-resolution transmission electron microscopy (HRTEM) and diffraction techniques, we demonstrate the coexistence of two (i.e., both *o*- and *t*-) Ge local environments. We emphasize the interplay between the unique defects in this alloy, i.e., the high-concentration CVs and *t*-Ge atoms, and the resulting consequences on the structure, stability, and properties of this material. The new structural model will be further validated by comparing with other experimental structural and property data.

$\text{Ge}_2\text{Sb}_2\text{Te}_5$ thin films about 30 nm in thickness were prepared by rf magnetron sputtering using a $\text{Ge}_2\text{Sb}_2\text{Te}_5$ alloy target and then annealed in a vacuum furnace for 2 hours at 200 °C to obtain polycrystalline *c*-GST. The selected area electron diffraction experiments were performed on a JEOL-2010 TEM operated at 200 kV, and HRTEM experiments were performed on FEI Titan 80–300 TEM with a Cs corrector operated at 300 kV. The diffraction intensity profiles were used in Fourier transforms to obtain the total radial distribution function (RDF). *Ab initio* total energy calculations were carried out by using the Vienna *ab initio* simulation package (VASP) [22] with the projected augmented plane-waves method [23,24] and the Perdew-Wang exchange-correlation functional [25]. The $3 \times 3 \times 3$ supercell used in the calculation contains 42 Ge, 44 Sb, 22 CVs, and 108 Te. The Γ point is used in the Brillouin zone sum.

Figure 1(a) shows a bright-field TEM image of the *c*-GST film and the corresponding selected area electron diffraction pattern (inset). The RDF extracted from the selected area electron diffraction intensity profile is presented in Fig. 1(b). Additional information is given in the supplemental information (Fig. S1) [26]. This approach

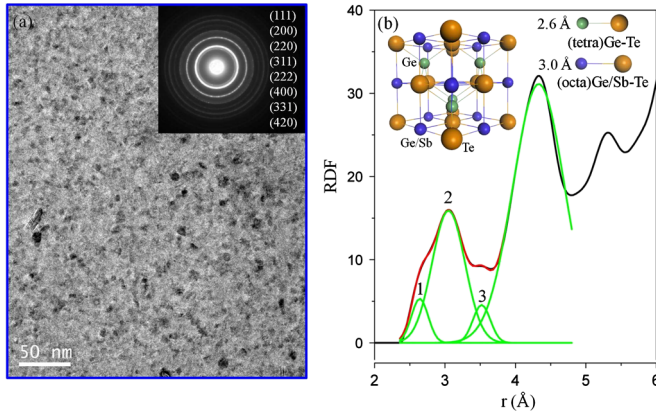


FIG. 1 (color online). (a) Bright-field image and diffraction pattern (inset) of polycrystalline metastable $\text{Ge}_2\text{Sb}_2\text{Te}_5$. (b) RDF based on the diffraction pattern in (a). The green lines are the Gaussian decomposition of the RDF. The inset shows a ball-stick model in which the Ge atoms occupy both tetrahedral (green) and octahedral (blue) sites.

allows us to use the bond lengths identified in the RDF to characterize the local Ge environments. Different from a perfect RS structure, two shoulder peaks are observed around the first peak in Fig. 1(b), in addition to the widely reported 3.01 Å RS peak [6,7]. Using the Gaussian peak splitting method and taking the peak at 4.3 Å as a reference, we identify the two shoulder peaks at 2.6 and 3.5 Å, respectively.

In a RS structure, the bond length between an o cation and Te is 3.01 Å and that between an interstitial t cation and Te is 2.61 Å. Therefore, the RDF suggests that the c -GST contains both o and t cations (Ge). The presence of t -Ge will be further verified by using HRTEM imaging, to be discussed later. The peak near 3.5 Å is originated from the distortion of RS framework (see Fig. S2 [26]).

The peak areas in Fig. 1(b) provide a quantitative measure of the number of t -Ge and Te bonds (the area underneath peak 1, A_1), as well as the o -Ge and Te bonds (the sum of the areas underneath peak 2 and peak 3, $A_2 + A_3$). The assignments of the peaks to specific bonds have been confirmed in our *ab initio* calculations (see below). Because the coordination number of t -Ge is 4 and that of o -Ge or o -Sb is 6, the following relationship holds:

$$4n_{t\text{-Ge}}/6(n_{o\text{-Ge}} + n_{\text{Sb}}) = A_1/(A_2 + A_3), \quad (1)$$

where $n_{t\text{-Ge}}$, $n_{o\text{-Ge}}$, and n_{Sb} are the number of t -Ge, o -Ge, and Sb, respectively. In addition, for $\text{Ge}_2\text{Sb}_2\text{Te}_5$

$$n_{t\text{-Ge}} + n_{o\text{-Ge}} = n_{\text{Sb}} = 0.4n_{\text{Te}}. \quad (2)$$

Using Eqs. (1) and (2) and the results in Fig. 1(b), we obtain $n_{t\text{-Ge}}/(n_{o\text{-Ge}} + n_{t\text{-Ge}}) \approx 0.34$. This ratio of the t -Ge to the total Ge ranges from 32% to 37% in several other samples measured. On average, about 35% Ge are on the fourfold t sites.

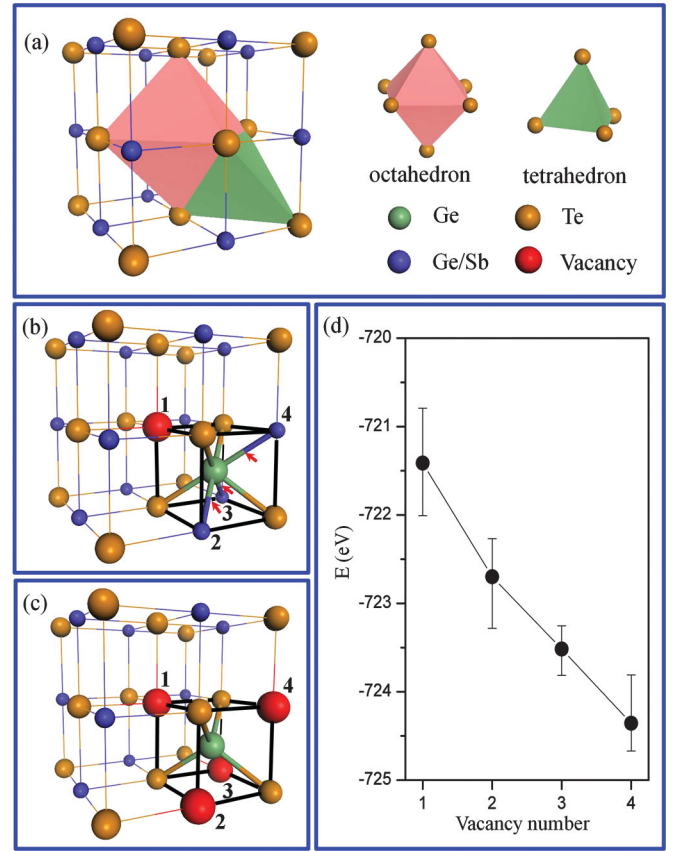


FIG. 2 (color). (a) A ball-stick model of the RS structure and the octahedral and tetrahedral cages enclosed by Te. (b) A local $V_t\text{GP}$ structure where wrong bonds between t -Ge and o -Ge/Sb are indicated by red arrows. (c) A local $V_4t\text{G}$ structure without any wrong bond. (d) Total energy of the local $V_n t\text{G}$ structures where $n = 1-4$. Three randomly chosen cation configurations are calculated, yielding an average (black data points).

To better determine and understand the atomic structure, we have employed *ab initio* calculations. Figure 2(a) shows an ideal RS structure in which an octahedron and a tetrahedron enclosed by Te atoms are highlighted. Note that a cation inside the tetrahedron has 8 nearest neighbors (NNs): 4 Te and 4 o cations. Thus, when one Ge atom is displaced from the octahedral position 1 to the tetrahedral position as shown in Fig. 2(b), it forms three wrong bonds. This is energetically unfavorable because Ge is covalent and would prefer a fourfold coordination [11–13]. The presence of the t -Ge would therefore provide the motivation for a rearrangement of the existing CVs towards t -Ge to lower energy [11–13], forming vacancy-interstitial t -Ge pairs ($V_t\text{GP}$). We have calculated the total energy for a set of configurations with one t -Ge surrounded by 1, 2, 3, or 4 CVs. Figure 2(d) shows that the total energy monotonically decreases with the increasing number of NN CVs, with 4 CVs [$V_4t\text{G}$ in Fig. 2(c)] being the most favorable.

Since every t -Ge desires more NN CVs, the t -Ge naturally aggregates to share the CVs in order for more of the 35% t -Ge to increase their surrounding CVs.

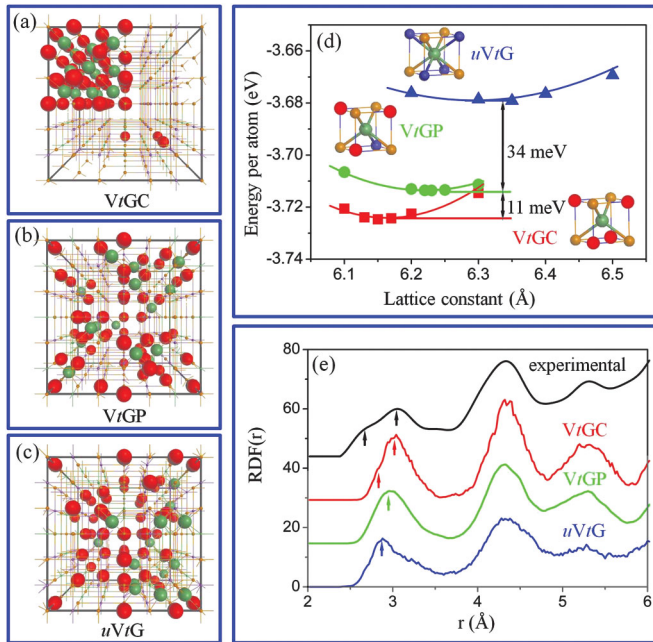


FIG. 3 (color). Configurations for (a) $VtGC$, (b) $VtGP$, and (c) $uVtG$. Red spheres are the CVs. (d) The corresponding total energy per atom as a function of lattice parameter a . (e) Experimental and simulated RDFs at room temperature (300 K). Arrows indicate peak positions in the RDFs.

This aggregation of $VtGPs$ to form their clusters ($VtGCs$) and hence domains, as modeled in Fig. 3(a), further suppresses the formation of wrong bonds between cation atoms, thereby lowering the system energy. This is compared with Figs. 3(b) and 3(c), which represent randomly distributed $VtGPs$ and a random distribution of totally uncorrelated CVs and t -Ge ($uVtG$), respectively. On average, there are 0, 1, and 3 wrong bonds per t -Ge for the $VtGC$, $VtGP$, and $uVtG$ configurations, respectively. Figure 3(d) compares the calculated total energy as a function of lattice parameter for these three cases (for structural details, see Fig. S3 [26]). We see that $VtGP$ and $uVtG$ are 11 and 45 meV/atom higher in energy than $VtGC$, respectively (which also has a lattice parameter closest to experiments [6,7]). This establishes that the $VtGC$ structure (with minimal wrong bond) is preferred for c -GST.

To compare with experimental structural information, we performed *ab initio* molecular dynamics simulations for the structural models, at 300 K in a 3 fs time step. Free energies stabilize after about 0.5 ps for all three models. Room-temperature RDFs are obtained by averaging the RDFs calculated for each model in the time interval between 0.5 and 3 ps, and the results are shown in Fig. 3(e). As indicated by the arrows, the RDF for $VtGC$ shows a shoulder at about 2.81 Å beside the 3.02-Å peak. In contrast, the RDF for $VtGP$ has only one peak at about 2.97 Å, whereas that for $uVtG$ has only one peak at about 2.87 Å. Hence, only the $VtGC$ model qualitatively agrees with experiment [also shown in Fig. 3(e)]. Figure S4 [26]

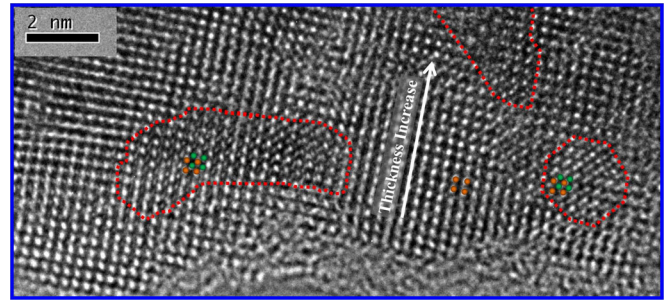


FIG. 4 (color online). Experimental Cs-corrected HRTEM images, taken along the [001] zone axis. The red-line-circled area consists of two sets of lattices (orange and green spheres), whereas the outer area has only one (orange spheres). Experimental conditions: voltage = 300 kV; Cs = -0.013 mm; and overfocus = 6 ± 1 nm.

decomposes the RDF for the $VtGC$, $VtGP$, and RS models. Not only the shoulder for $VtGC$ in Fig. 3(e) can be clearly resolved but the peaks at 3.5 Å can also be clearly attributed to distorted RS (cf. Fig. S2 [26]), not to tetrahedrally coordinated Ge.

In addition, we have calculated the Ge-edge x-ray-absorption near-edge structure spectra for the $VtGC$ model, as well as for the quenched amorphous states. They are found to agree very well with the experimental x-ray-absorption near-edge structure data [11] (see Fig. S5 [26]). The standard x-ray diffraction techniques, used in previous studies, cannot differentiate between the RS model and the $VtGC$ model either, as both exhibit practically the same powder x-ray diffraction pattern. Both are in good agreement with experiment (see Fig. S6 [26]).

All the evidences above are consistent with the picture that a $VtGC$ structure is more likely what is actually present in the GST, rather than the structure crudely depicted by the RS model. A direct confirmation of this conclusion, however, comes from HRTEM imaging; see Fig. 4. Note that an important prediction of the $VtGC$ model is the existence of many t -Ge atoms and domains where t -Ge atoms are populous. These tetrahedral atoms and domain structures are clearly observed in the area circled by red dots in Fig. 4. The enclosed areas show two sets of lattices (marked by two sets of colored spheres), with one set in the tetrahedral positions. The areas outside the enclosures have only one set of lattice consistent with RS. Along the thickness direction, these t -Ge domains are randomly distributed with RS regions. This indicates that the domain structure is not the “fake image” induced by a thickness change. In addition, the domains (about 2–6 nm in equivalent diameter) have no regular shapes and they are usually isolated by RS regions. Figures S7(a)–(c) [26] show the simulated HRTEM images based on the various models; here again only the $VtGC$ model qualitatively agrees with experiments.

Another supporting evidence is the calculated optical properties of the $VtGC$ model, as compared with those of

the RS and amorphous structures (for details, see Fig. S8 [26]). The optical absorption ε_2 is about 40 for the VtGC model, lower than that of 50 for the RS model but in better agreement with experiment. The lowering of ε_2 in the VtGC model can be expected because a considerable amount of tetrahedrally coordinated Ge atoms would disrupt resonant bonding to reduce the contrast [10].

Based on this new understanding of the coexistence of octahedral and tetrahedral Ge in *c*-GST, and the amorphous structure which has been resolved recently [27–29], we believe that the phase-change mechanism of GST is distinctly different from the previously proposed umbrella-flip model [11]. Upon amorphization or crystallization, the basic NN structural motifs of the octahedral and tetrahedral Ge atoms remain largely intact; i.e., $\sim 30\%$ Ge are in the tetrahedral locations and the rest in the octahedral environments (similar proportions are known for the local structures in the amorphous phase [27–29]). No medium and long-range diffusion process is needed. Even the short-range “umbrella flip” between tetrahedral and octahedral sites is not necessary (a recent investigation has indicated the dominance of *p* bonding in the amorphous phase [29], which also indicates that the umbrella-flip phase transition model [11] needs to be evaluated). The phase-change (e.g., crystallization) process can thus be extremely fast, when the preexisting octahedral and tetrahedral Ge-centered local motifs and clusters rearrange, by restoring periodicity, adjusting bond lengths, and eliminating excess space to assemble into the cubic phase. Meanwhile, the distinctive optical absorption differences in Fig. S8 [26] arise mainly from the presence (versus absence) of the medium and long-range ordering of the crystalline lattices and the different contents of vacancies (excess volume) in the crystalline and amorphous states.

In conclusion, by measuring and analyzing the RDF of *c*-GST, we identify the coexistence of local *t*- and *o*-Ge and determine that the amount of *t*-Ge is about 1/3 of the total Ge. *Ab initio* calculations further reveal that cation vacancies play a pivotal role in stabilizing the tetrahedral coordination by forming CV and *t*-Ge pairs and subsequently their clustering into domains when the pairs share the CVs. The similarity of local structure around Ge atoms in both the cubic and amorphous phases would render the phase change diffusionless, contribute to the fast switching between the two states, and promote the reversibility of the phase transition.

This work was supported by the National Basic Research Program of China (2007CB935400, 2009CB623700),

National Outstanding Young Scientist Grant of China (No. 10825419), and the Key Project of C-NSF (No. 50831001). S. B. Z. is supported by U.S. DOE under Grant No. DE-SC0002623. Y. Q. C., M. X., and E. M. are supported at JHU by U.S. DOE-MS&E under Contract No. DE-FG02-09ER46056. The HRTEM work made use of the resources of the Beijing National Center for Electron Microscopy.

*xdhan@bjut.edu.cn

†zhangs9@rpi.edu

‡ema@jhu.edu

- [1] M. Wuttig and N. Yamada, *Nature Mater.* **6**, 824 (2007).
- [2] S. R. Ovshinsky, *Phys. Rev. Lett.* **21**, 1450 (1968).
- [3] J. Feinleib *et al.*, *Appl. Phys. Lett.* **18**, 254 (1971).
- [4] N. Yamada *et al.*, *J. Appl. Phys.* **69**, 2849 (1991).
- [5] T. Ohta, *J. Optoelectron. Adv. Mater.* **3**, 609 (2001).
- [6] N. Yamada and T. Matsunaga, *J. Appl. Phys.* **88**, 7020 (2000).
- [7] T. Nonaka *et al.*, *Thin Solid Films* **370**, 258 (2000).
- [8] S. Hosokawa *et al.*, *Appl. Phys. Lett.* **90**, 131913 (2007).
- [9] T. Matsunaga, N. Yamada, and Y. Kabota, *Acta Crystallogr. Sect. B* **60**, 685 (2004).
- [10] K. Shportko *et al.*, *Nature Mater.* **7**, 653 (2008).
- [11] A. V. Kolobov *et al.*, *Nature Mater.* **3**, 703 (2004).
- [12] W. Welnic *et al.*, *Nature Mater.* **5**, 56 (2006).
- [13] W. Welnic *et al.*, *Phys. Rev. Lett.* **98**, 236403 (2007).
- [14] J. Hegedus and S. R. Elliott, *Nature Mater.* **7**, 399 (2008).
- [15] C. Steimer *et al.*, *Adv. Mater.* **20**, 4535 (2008).
- [16] J. J. Kim *et al.*, *Phys. Rev. B* **76**, 115124 (2007).
- [17] Z. Sun, J. Zhou, and R. Ahuja, *Phys. Rev. Lett.* **96**, 055507 (2006).
- [18] M. Wuttig *et al.*, *Nature Mater.* **6**, 122 (2007).
- [19] A. V. Kolobov *et al.*, *Phys. Rev. Lett.* **97**, 035701 (2006).
- [20] Z. Sun *et al.*, *Phys. Rev. Lett.* **102**, 075504 (2009).
- [21] S. Caravati *et al.*, *Phys. Rev. Lett.* **102**, 205502 (2009).
- [22] G. Kresse and J. Furthmüller, *Comput. Mater. Sci.* **6**, 15 (1996).
- [23] P. E. Blöchl, *Phys. Rev. B* **50**, 17953 (1994).
- [24] G. Kresse and D. Joubert, *Phys. Rev. B* **59**, 1758 (1999).
- [25] Y. Wang and J. P. Perdew, *Phys. Rev. B* **44**, 13298 (1991).
- [26] See supplementary material at <http://link.aps.org/supplemental/10.1103/PhysRevLett.106.025501> for the detailed and intensive information.
- [27] S. Caravati *et al.*, *Appl. Phys. Lett.* **91**, 171906 (2007).
- [28] A. Klein *et al.*, *Phys. Rev. Lett.* **100**, 016402 (2008).
- [29] M. Xu *et al.*, *Phys. Rev. Lett.* **103**, 195502 (2009).